M. Carini, F. Auteri, F. Giannetti
Secondary Instabilities of the In-Phase Synchronized Wakes Past Two Circular Cylinders in Side-By-side Arrangement
Journal of Fluids and Structures, Vol. 53, 2015, p. 70-83
doi:10.1016/j.jfluidstructs.2014.09.004

Secondary instabilities of the in-phase synchronized wakes past two circular cylinders in side-by-side arrangement

M. Carini[a], F. Auteri[a,*], F. Giannetti[b]

[a]*Dipartimento di Scienze e Tecnologie Aerospaziali, Politecnico di Milano, via La Masa 34, 20156 Milano, Italy.*
[b]*Dipartimento di Ingegneria Industriale, Università degli Studi di Salerno, via Ponte don Melillo 1, 84084 Fisciano (SA), Italy.*

Abstract

In the present study we investigate the secondary instability of the in-phase synchronized vortex shedding from two side-by-side circular cylinders at low Reynolds numbers. Two distinct Floquet modes become unstable for different values of the Reynolds number and of the non-dimensional gap spacing, leading to the onset of the well-known *flip-flop* instability of the two cylinder wakes. In both cases the two-dimensional Floquet analysis reveals that at very low Reynolds numbers, a pair of complex-conjugate multipliers crosses the unit circle, showing the same frequency as the biased gap-flow flip-over. In the past literature this behaviour has been often ascribed to a bi-stability of the flow. On the contrary, the present DNS and stability results provide evidence that, at low Reynolds numbers, the flip-flopping behaviour originates from a Neimark-Sacker bifurcation of the in-phase shedding cycle.

Keywords:
Secondary instabilities, Floquet stability analysis, two side-by-side cylinders, flip-flop.

1. Introduction

Bluff body wake interaction plays an important role in several industrial applications, such as, for instance, in the flow past tube bundles in heat exchangers or in the design of high-rise buildings. A simple, yet interesting prototype of this kind of flows is represented by the incompressible flow past two side-by-side circular cylinders (Zdravkovich, 1977). In this configuration, the two cylinders are aligned along the direction perpendicular to the free stream (see Fig. 1) and the flow is governed by two independent non-dimensional parameters: the Reynolds number $\mathrm{Re} = U^*_\infty D^*/\nu$ and the non-dimensional distance between the cylinder surfaces $g = g^*/D$, U^*_∞ being the free-stream velocity, D^* the cylinder diameter and ν the kinematic viscosity. As the gap size is varied, basically three distinct vortex shedding regimes are observed: the single bluff-body regime ($g \lesssim 0.2$), the asymmetric regime ($0.2 \lesssim g \lesssim 1.2$) and the symmetric regime ($1.2 \lesssim g \lesssim 5$) with a synchronization of the vortex shedding from the two cylinders (Sumner, 2010). The synchronization may occur either in phase, leading to an anti-symmetric wake pattern, or in phase opposition resulting in a wake pattern symmetric with respect to the flow centerline. At low Reynolds numbers both these synchronized patterns have been described in the experimental work of Williamson (1985). In particular, while the symmetric double vortex street configuration is intrinsically more persistent and survives at larger distance from the two cylinders, the idealized anti-symmetric pattern rapidly evolves into a single large-scale street called *binary vortex* street (Williamson, 1985).

Among the various wake patterns that characterize the considered flow, we are particularly interested in the so called *flip-flopping* pattern that mainly arises in the asymmetric regime. Within this regime, a biased vortex shedding takes place from the two cylinders, the gap flow between them being deflected toward one of the two cylinder surfaces. In some cases the gap flow direction alternatively switches from one side to the other, which is commonly referred to as the flip-flopping behaviour. This phenomenon has been observed in several experiments (Bearman and Wadcock,

*Corresponding author
Email address: franco.auteri@polimi.it (F. Auteri)

1973; Kim and Durbin, 1988; Sumner et al., 1999; Zhou et al., 2002; Wang et al., 2002) and in numerical simulations (Kang, 2003; Chen et al., 2003; Afgan et al., 2011). For relatively high Reynolds numbers, the gap flow changes direction in an apparently random way as described by Kim and Durbin (1988) for $g = 0.75$ and $\mathrm{Re} = 2 - 7 \times 10^3$ or by Zhou et al. (2002) for $g = 0.5$ and $\mathrm{Re} = 5800$. At low Reynolds numbers the occurrence of the flip-flopping has been described by Kang (2003) using two-dimensional numerical simulations. Kang (2003) found that during the flip-flopping regime the drag coefficient of each cylinder slowly changes over a time scale one order of magnitude greater than that of vortex shedding, which is much smaller compared to the high Reynolds number case. Two parameter ranges have been described by the author for the occurrence of the flip-flopping: one main region at intermediate gap spacing $0.4 \lesssim g \lesssim 1.4$ for $\mathrm{Re} > 50$ and one smaller region at larger gap spacing $1.4 \lesssim g \lesssim 2.2$ for $50 \lesssim \mathrm{Re} \lesssim 70$ where the flip-flopping is found to coexists with the in-phase synchronized pattern. For $g = 0.7$ and $\mathrm{Re} = 150$ and 230 the flip-flop of the gap flow has been experimentally described by Wang et al. (2002), who provided a detailed analysis of the vortex dynamics associated with the switch-over phase by means of flow visualizations.

In the past literature, a bi-stability conjecture has been often invoked to explain the onset of the flip-flopping (Le Gal et al., 1994; Peschard and Le Gal, 1996). In these works the authors proposed a system of two coupled Landau equations to model the interactions between the two side-by-side cylinder wakes. Besides in-phase and anti-phase synchronized states, the model shows the existence of dual asymmetric locked solutions with a non-trivial phase difference and amplitude ratio between the two oscillators. Based on these results, the authors suggested that the flip-flop can be interpreted as the alternate switching between these dual asymmetric solutions, driven by external perturbations. This hypothesis has been further supported by Mizushima and Ino (2008), who showed that in a narrow range of gap spacing ($0.594 \leq g \leq 0.607$) the steady base flow past the two cylinders bifurcates to an asymmetric steady state, thus providing a rationale for such interpretation. Recently the global stability analysis of the steady symmetric base flow has been considered by Carini et al. (2014b), showing that this pitchfork bifurcation occurs for a remarkably wider interval of the gap width ($0.566 \leq g \leq 0.725$). Notwithstanding, for low Reynolds numbers, the bi-stability conjecture is not convincing. In fact, the second small parameter region where the emerging of the flip-flopping has been documented by Kang (2003) falls outside the gap spacing range of bifurcated asymmetric states (Carini et al., 2014b). Furthermore, within the second parameter region reported by the former author, the co-existence of both the in-phase and the flip-flopping states suggests us that the latter could arise from a secondary, two-dimensional instability of the in-phase shedding cycle through a subcritical bifurcation.

Based on two-dimensional DNS and stability analyses, we show that at low Reynolds numbers and for $0.6 \lesssim g \leq 2.4$ the flip-flopping behaviour originates from a Neimark–Sacker bifurcation of the in-phase vortex shedding cycle, leading to a torus in the phase space. For both the in-phase synchronized and the flip-flopping wake patterns, a different vortex dynamics is observed between $g = 0.7$ and $g = 1.8$, thus indicating that different physical mechanisms are involved at intermediate and large gap spacing. Correspondingly two distinct unstable Floquet modes breaking the spatio-temporal symmetry of the periodic base flow are found, both characterized by the low-frequency of the respective gap flow flip-over. Their corresponding instability domain is described in the parameter plane (g, Re). In addition a weakly nonlinear analysis in the neighbourhood of the double Hopf bifurcation point at $g_c = 1.875$ and $\mathrm{Re}_c = 51.51$ (Carini et al., 2014b) is performed to get further insight in the nature of the flip-flop instability at large gap spacing.

The work is organized as follows. The flow configuration and the governing equations are introduced in §2 along with some details about the Floquet stability analysis. The employed numerical procedures are summarized in §3. DNS results are reported in §4 where the flip-flopping vortex dynamics is investigated. Then the stability analysis is presented in §5. The periodic base flow is illustrated in §5.1, for both $g = 0.7$ and $g = 1.8$. Then the domains of instability of the two Floquet modes are described in §5.2 and their spatio-temporal structures are presented in §5.3 for both $g = 0.7$ and $g = 1.8$. Finally the normal-form of the double Hopf bifurcation is analyzed in §5.4 and some conclusions are drawn in §6.

2. The mathematical problem

The present study deals with the incompressible flow of a Newtonian fluid of constant density ρ^* around two identical circular cylinders in side-by-side arrangement. With reference to Fig. 1, the cylinder centres are aligned on the y-axis and symmetrically placed with respect to the x-axis which is oriented as the free-stream velocity. The

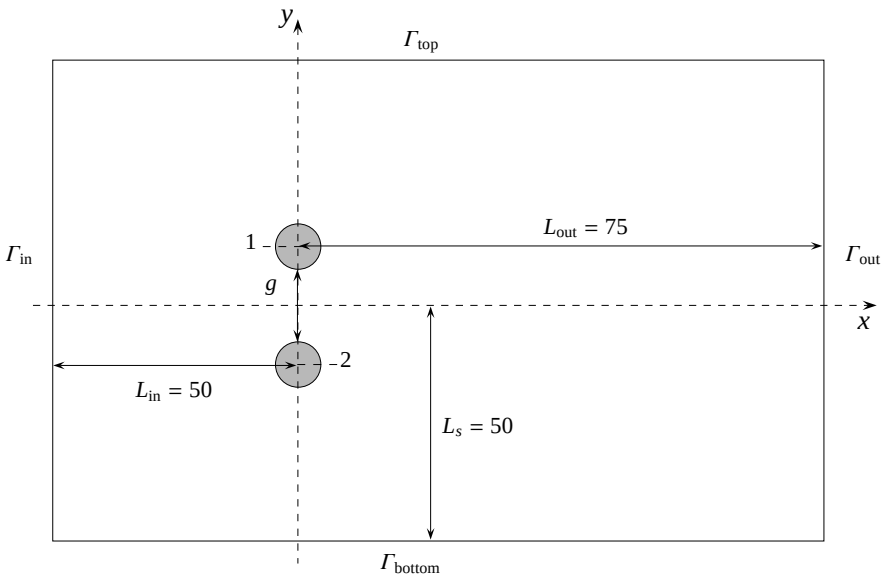

Figure 1: Sketch of the flow configuration and of the computational domain Ω_c.

governing incompressible Navier–Stokes equations made dimensionless using D^*, U^*_∞ and ρ^* are written as:

$$\begin{cases} \dfrac{\partial \boldsymbol{U}}{\partial t} + (\boldsymbol{U}\cdot\boldsymbol{\nabla})\boldsymbol{U} = -\boldsymbol{\nabla}P + \dfrac{1}{\mathrm{Re}}\nabla^2\boldsymbol{U}, \\ \boldsymbol{\nabla}\cdot\boldsymbol{U} = 0, \end{cases} \tag{1}$$

where $\boldsymbol{U}$ is the velocity field with components $\boldsymbol{U} = (U, V)$ and P is the reduced pressure. At the outlet boundary Γ_{out} the above equations are supplemented with the boundary conditions $-P + 2\mathrm{Re}^{-1}\partial U/\partial x = 0$ and $\partial V/\partial x = 0$. Both at the inlet Γ_{in} and at the side boundaries Γ_{top} and Γ_{bottom}, the vorticity is set to zero and the flow perturbation produced by the two cylinders on the incoming uniform stream is assumed to decay to zero as the leading term in the potential flow around them. No-slip conditions are imposed on the cylinder surfaces.

2.1. Floquet analysis

As already mentioned we are interested in the two-dimensional Floquet analysis of the in-phase synchronized vortex shedding from the two cylinders. For such purpose, the total flow field $\boldsymbol{Q} = \{\boldsymbol{U}, P\}$ is decomposed as the sum of the periodic base flow, $\boldsymbol{Q}_b = \{\boldsymbol{U}_b, P_b\}$, of period T and of a small, unsteady perturbation, $\boldsymbol{q} = \{\boldsymbol{u}, p\}$, i.e. $\boldsymbol{Q}(x, y, t) = \boldsymbol{Q}(x, y, t) + \epsilon\boldsymbol{q}(x, y, t)$, ϵ being the amplitude of the perturbation, with $\epsilon \ll 1$. Since we are concerned with the stability properties of the periodic base flow, without loss of generality, the total perturbation field can be written in the form $\boldsymbol{q}(x, y, t) = \hat{\boldsymbol{q}}(x, y, t)\exp(\sigma t)$ where $\sigma \in \mathbb{C}$ is the Floquet exponent and $\hat{\boldsymbol{q}} = \{\hat{\boldsymbol{u}}, \hat{p}\}$ denotes a non-trivial, periodic, complex-valued field having the same period T of the base flow. By introducing the above decomposition in the Navier–Stokes equations (1) and getting rid of second-order terms in ϵ, we obtain the following eigenvalue problem:

$$\begin{cases} \dfrac{\partial \hat{\boldsymbol{u}}}{\partial t} + \sigma\hat{\boldsymbol{u}} + (\boldsymbol{U}_b\cdot\boldsymbol{\nabla})\hat{\boldsymbol{u}} + (\hat{\boldsymbol{u}}\cdot\boldsymbol{\nabla})\boldsymbol{U}_b - \dfrac{1}{\mathrm{Re}}\nabla^2\hat{\boldsymbol{u}} + \boldsymbol{\nabla}\hat{p} = \boldsymbol{0}, \\ \boldsymbol{\nabla}\cdot\hat{\boldsymbol{u}} = 0. \end{cases} \tag{2}$$

For the above set of equations the same boundary conditions introduced so far are applied with homogeneous data. In addition, a time periodicity constraint is imposed on $\hat{\boldsymbol{q}}(t)$. For a given Reynolds number and gap spacing, the flow is unstable if there exists a non-trivial solution $\hat{\boldsymbol{q}}$ whose associated Floquet exponent has real part greater than zero.

	$\bar{C}_D$	C'_L	St
Kang (2003)	1.434	0.271	0.164
Present (M_0)	1.409	0.262	0.163
Present (M_F)	1.408	0.266	0.163

Table 1: Comparison of DNS results for the in-phase synchronized vortex shedding from the two cylinders at $g = 1.5$ and Re $= 100$, being $\bar{C}_D$ the mean drag coefficient, C'_L the maximum amplitude of the lift coefficient fluctuations and St the Strouhal number. Due to vortex shedding synchronization, all these quantities assume the same value for both cylinders. The present computations have been performed on both the grid denoted by M_0 and the finer grid denoted by M_F.

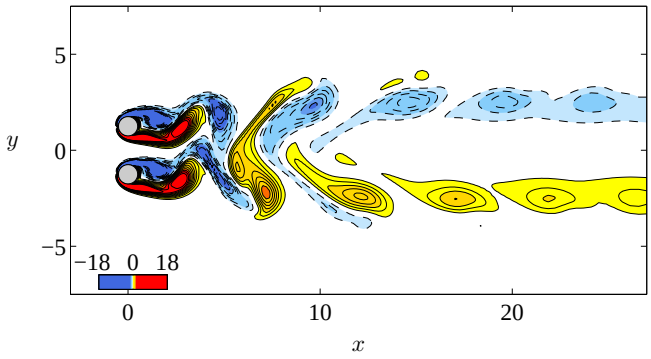

Figure 2: Flow vorticity snapshot during the in-phase synchronized vortex shedding at $g = 1.5$ and Re $= 100$.

3. Numerical approach

Both the two-dimensional DNS and the Floquet stability analysis have been carried out on the domain Ω_c reported in Fig. 1. The computational domain extends for a length $L_x = 125$ in the x direction and $L_y = 100$ in the y direction. The inlet (outlet) is located at 50 (75) diameters from the cylinder centres. On Ω_c the Navier–Stokes equations are discretized by a second-order finite difference scheme on staggered Cartesian grids and the cylinder surfaces are treated according to the immersed boundary technique reported in Giannetti and Luchini (2007). A total of 430×450 grid nodes has been employed, the grid being refined near the cylinder surfaces up to the smallest size of 0.02 in both directions x and y. Such grid will be referred to as M_0. The third-order Runge-Kutta/Crank-Nicolson scheme proposed by Rai and Moin (1991) has been used to advance the equations in time, treating the Stokes operator implicitly and the convective terms explicitly. In this way, the linear system arising from the spatial discretization can be factored once and for all in the preprocessing phase. The LU solver UMFPACK (Davis, 2004) has been employed for this task. For time integration, a non-dimensional time step $\Delta t = 0.03$ has been used. Finally, the least stable Floquet modes have been computed by repeatedly marching the linearized system (2) over the period T and using the Arnoldi algorithm implemented in the ARPACK library (Lehoucq et al., 1998); see Giannetti et al. (2010) and Camarri and Giannetti (2010) for further details.

A DNS convergence check, employing 700×800 points (grid M_F) and a time step $\Delta t = 0.015$, has been also performed showing that the present results are converged up to three significant digits. As an example the DNS results obtained for $g = 1.5$ and Re $= 100$ are compared with those of Kang (2003) in Table 1, showing good overall agreement. A vorticity snapshot of the flow field illustrating the in-phase vortex shedding from the two cylinders is reported in Fig. 2.

4. DNS results

Several simulations have been performed for $g = 0.7$ and $g = 1.8$ while varying the Reynolds number in the range $50 <$ Re < 70. All the simulations have been started from a random velocity field and have been continued

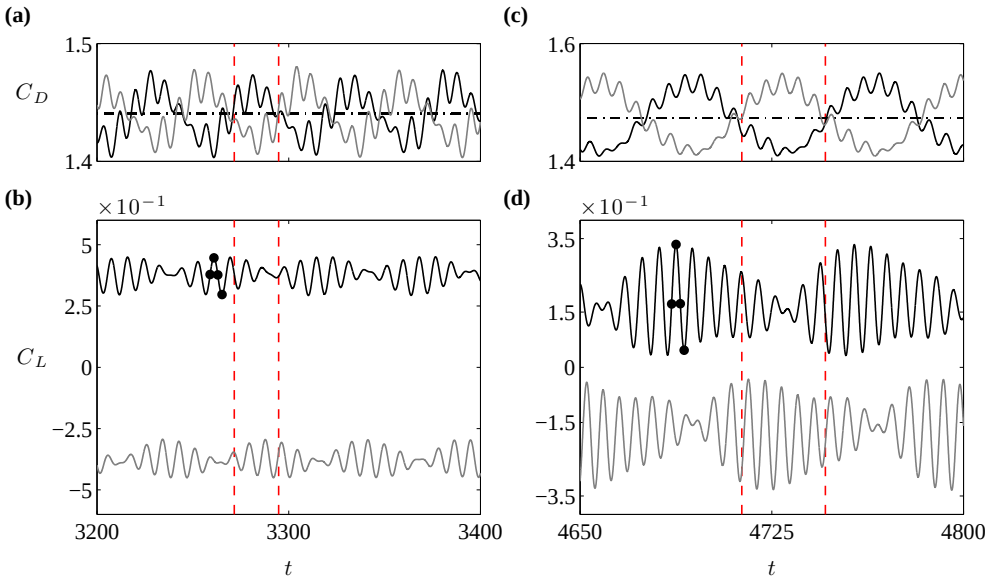

Figure 3: Time series of the lift and drag coefficients for the upper (1) and lower cylinder (2) (see Fig. 1) during the fully developed flip-flopping regime: $C_{L,1}$, $C_{D,1}$ black lines, $C_{L,2}$, $C_{D,2}$ grey lines. (a,b) $g = 0.7$ and Re = 68.8. (c,d) $g = 1.8$ and Re = 63. In Fig. (b) and (d) round dots are used to mark the shedding phases corresponding to the vorticity snapshots which are reported in Fig. 6, on the right and left column, respectively. Dashed vertical lines approximately indicate two subsequent gap flow flip-overs marked by square dots in Fig. 5(a) and 5(b).

up to ≈ 5000 nondimensional time units. The time traces of the lift and drag coefficients corresponding to the fully developed flip-flopping regime are illustrated in Fig. 3(a) for Re $= 68.8$ at $g = 0.7$ and in Fig. 3(b) for Re $= 63$ at $g = 1.8$. In both cases the C_L time series show a characteristic beating like waveform: their relative phase is no more constant but changes with time and the related period is not a multiple or sub-multiple of the vortex shedding frequency. Correspondingly, the related C_D time traces appear as the superposition of a relatively high frequency signal, which corresponds to the in-phase vortex shedding, modulated in amplitude by a low frequency signal which is shown to be related to the alternate deflection of the gap flow.

The spectrum of the lift coefficient fluctuations for the case at $g = 0.7$ is illustrated in Fig. 4(a) showing three well-defined peaks. The main peak $\mathrm{St}_2 = 0.1119$ corresponds to the in-phase vortex shedding, while the lowest frequency peak $\mathrm{St}_1 = 0.0193$ is related to the oscillation of the gap flow direction and is in good agreement with the value reported by Kang (2003) for Re $= 100$ and $g = 1$ (St $= 0.018$). The third peak is most probably produced by a nonlinear interaction of the other two modes since $\mathrm{St}_3 \approx \mathrm{St}_1 + \mathrm{St}_2$. Similar considerations apply to the spectrum computed for $g = 1.8$, see Fig. 4(b). In this case up to six strong peaks can be distinguished. The lowest frequency one ($\mathrm{St}_1 = 0.0137$) is still related to the unsteady deflection of the gap flow. Of the remaining five, the central one ($\mathrm{St}_4 = 0.1437$) corresponds to the vortex shedding frequency while the other four result from the nonlinear interaction between St_4 and St_1. Indeed $\mathrm{St}_2 = 0.1160 \approx \mathrm{St}_4 - 2\mathrm{St}_1$, $\mathrm{St}_3 = 0.1297 \approx \mathrm{St}_4 - \mathrm{St}_1$, $\mathrm{St}_5 = 0.1577 \approx \mathrm{St}_4 + \mathrm{St}_1$ and $\mathrm{St}_6 = 0.1714 \approx \mathrm{St}_4 + 2\mathrm{St}_1$.

In order to investigate the relationship between the aerodynamic forces acting on the cylinders and the deflection of the gap flow, the time history of the V component of the velocity field at $(x, y) = (0.5, 0)$ is illustrated in Fig. 5. For both $g = 0.7$ and $g = 1.8$, the sign of $V(0.5, 0, t)$, which provides an indication of the direction of the gap flow, changes at a frequency which is one order of magnitude lower than that of the vortex shedding and corresponds to the lowest frequency peak observed in the spectrum of the C_L. Therefore, the gap flow remains weakly deflected toward one of the cylinders for more than one vortex shedding period. According to the signals of Fig. 5, the flip-over time instants (square dots) approximately correspond to the phase at which the drag coefficient fluctuations change sign, as indicated by dashed vertical lines in Fig. 3. Moreover, it can be noticed that an higher drag coefficient is experienced by the cylinder towards which the gap flow is deflected which is a general feature of the asymmetric vortex shedding regime (Sumner, 2010).

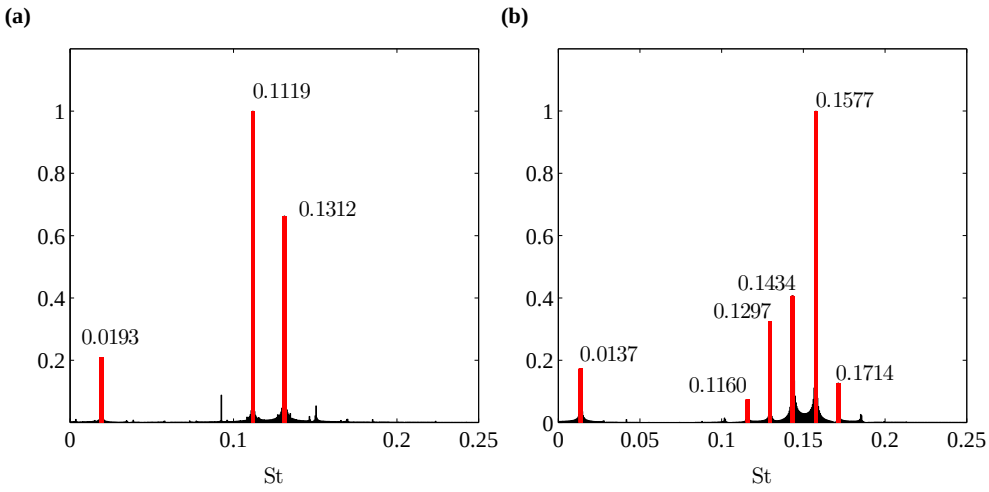

Figure 4: Spectral content of the lift coefficient associated with the flip-flopping behaviour. (a) $g = 0.7$ and Re = 68.8. (b) $g = 1.8$ and Re = 63.

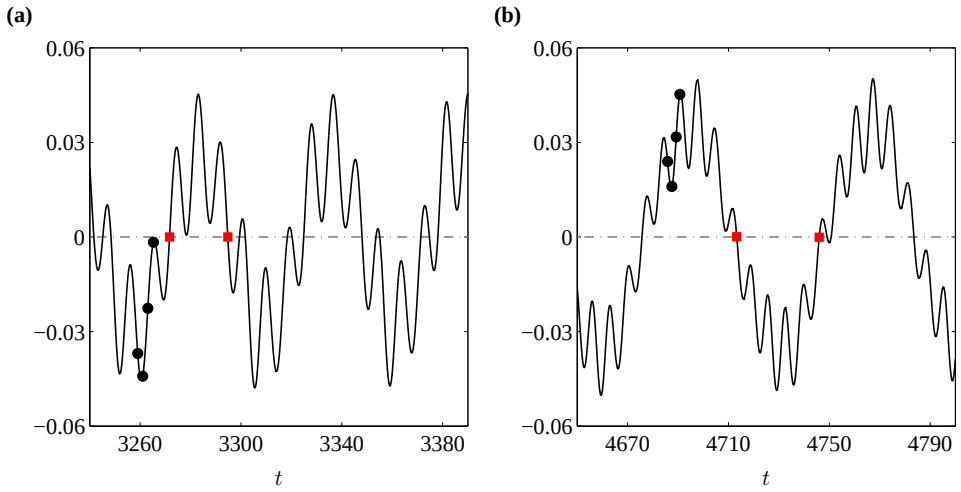

Figure 5: Time history of the cross-stream velocity component $V(x_p, y_p, t)$ at $(x_p, y_p) = (0.5, 0)$ during the flip-flopping regime. (a) $g = 0.7$ and Re = 68. (b) $g = 1.8$ and Re = 63. Black round dots refer to vorticity snapshots in Fig. 6 (see also Fig. 3) while the two square dots approximately indicate two subsequent switching phases of the gap flow deflection.

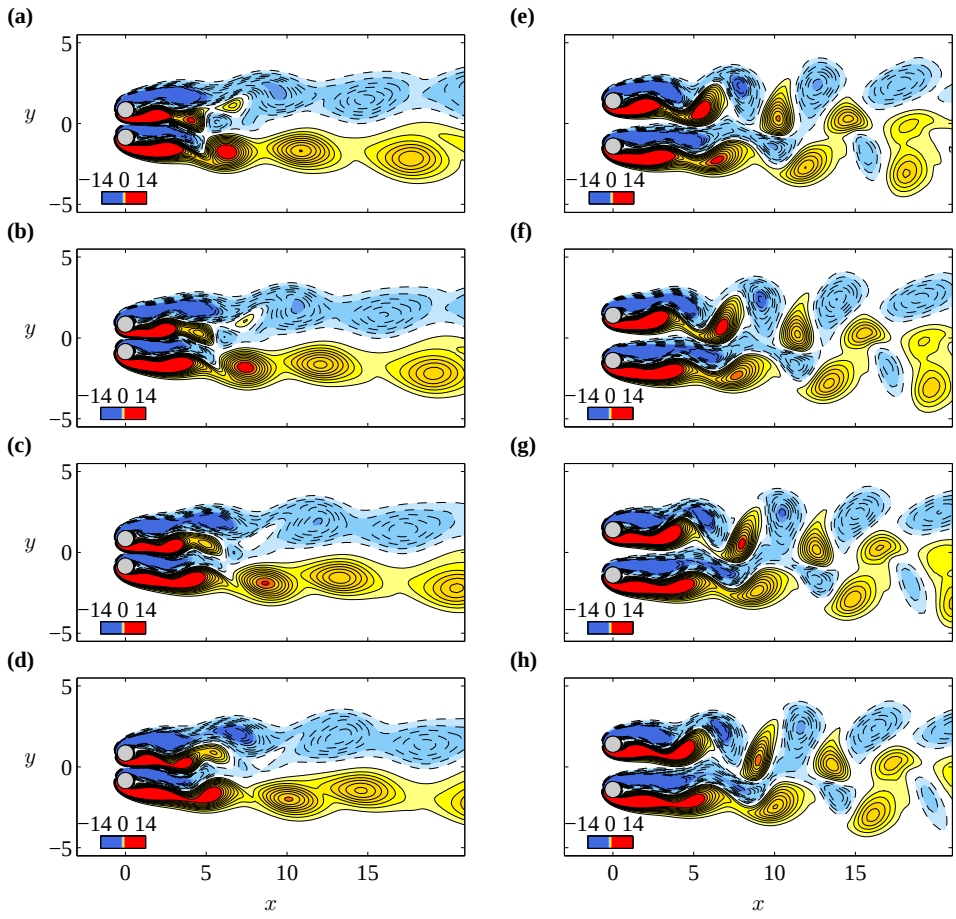

Figure 6: Vorticity snapshots of the fully developed flip-flopping flow for $g = 0.7$ and Re = 68.8 (left column) and for $g = 1.8$ and Re = 63 (right column). Black round dots are used in Fig. 3 and 5 to mark shedding phases corresponding to the above snapshots. For (a)–(d) a weakly downward deflection of the gap flow is observed. On the contrary for (e)–(h) the gap flow is weakly deflected upward.

The flip-flopping behaviour can be better understood by inspecting the vortex dynamics for the two considered values of the gap spacing. Almost the same phases during one shedding cycle are depicted in Fig. 6 for both cases. These shedding phases are marked by round black dots in Fig. 3 and 5. For $g = 0.7$, Fig. 6(a)–(d), larger vortices are shed from the outer shear layers of the two cylinders while smaller vortices develop from the inner shear layers. During one shedding cycle, the two gap eddies merge into the outer vortex street on the same side with the formation of a narrow and a wide wake behind the two cylinders while a single large-scale vortex street is formed in the far wake. A similar vortex dynamics has been reported by Williamson (1985) while investigating the asymmetric vortex shedding regime for $g = 0.85$ and $\mathrm{Re} = 200$. The merging direction of the gap vortices is not fixed but changes with time according to the switch-over of the gap flow which is weakly deflected downward in the snapshots of Fig. 6(a)–(d). For $g = 1.8$, Fig. 6(e)–(h), the vortex dynamics is completely different. In this case two distinct vortex streets develop from the cylinders and a vortex merging process similar to that characterizing the evolution of the binary vortex street is observed. An example of such transition is depicted in Fig. 2 for $g = 1.5$ and $\mathrm{Re} = 100$: during the in-phase vortex shedding regime, like-signed vortices shed at the same time pair up, merge and rotate around each other leading to the formation of two counter rotating vortex rows on opposite sides of the flow centerline, a wake pattern for which the term *binary street* was introduced by Williamson (1985). During the flip-flop at $g = 1.8$ this mechanism occurs only on one side of the wake. This is shown in Fig. 6(e)–(h) where only counter-clockwise rotating vortices are observed to merge, while the same does not happen for opposite sign vortices. In particular on the outer, bottom side of the two cylinder wakes, each gap vortex shed from the lower cylinder remains trapped between pairs of merging eddies, which prevents the formation of the binary vortex street structure. In analogy with the case at $g = 0.7$, as the gap flow deflection switches from upward to downward, the biased pairing process occurs only for negative sign vortices on the upper wake side. A similar asymmetric wake pattern has been described by Le Gal (1991) by means of flow visualization for $g = 4$ and $\mathrm{Re} = 110$.

5. Stability results

Contrary to what previously conjectured by other authors, the spectra reported in Fig. 4 and the highlighted analogies with the in-phase vortex dynamics for the flip-flopping at $g = 1.8$, suggest that the flip-flopping behaviour could originate as a secondary instability of the in-phase vortex shedding cycle. In order to assess this novel interpretation, a two-dimensional Floquet stability analysis of the in-phase periodic base flow has been performed.

5.1. Periodic base flow

The periodic base flow corresponding to the in-phase vortex shedding limit cycle is illustrated in Fig. 7 and 8 for $g = 1.8$ ($\mathrm{Re} = 54$) and $g = 0.7$ ($\mathrm{Re} = 61.6$), respectively. For $g = 1.8$, the base flow displays the same wake structure which has been described by several authors with the characteristic formation of the binary vortex street in the far field (Williamson, 1985; Sumner et al., 1999; Kang, 2003). At low Reynolds numbers this flow pattern can been obtained from DNS in the range of $1.5 \lesssim g \lesssim 5$ (Kang, 2003). Conversely, when reducing the gap width at $g = 0.7$, Fig. 8, the resulting in-phase pattern appears still characterized by the formation of a single large scale vortex street, but the underlying vortex dynamics is different from the aforementioned one. During one period, each small gap eddy is transported between two subsequent big vortices shed from the outer shear layer on the opposite cylinder side. Thus gap vortices merge on opposite sides of the outer large scale street. In Fig. 9(a) the in-phase synchronization of the two wakes for $g = 0.7$ is confirmed by the superposition of the time traces of the lift coefficient fluctuations of the two cylinders $\Delta C_{L,1-2}$. In addition black round dots are used to mark the shedding phases corresponding to base flow snapshots in Fig. 8. The same definition of the shedding phases have also been used for the case at $g = 1.8$, Fig. 7. In Fig. 9(b), the signal $V(0.5, 0, t)$ associated with the periodic base flow for $g = 0.7$ and $\mathrm{Re} = 61.6$ shows that gap flow oscillations are periodic and synchronized with the vortex shedding frequency, as expected. The same behaviour holds for the case at $g = 1.8$ (not shown here).

It is worthwhile to note that in both cases the T-periodic *in-phase* base flow obeys the reflection symmetry about the x-axis when time is advanced of $T/2$: this is clearly highlighted by selected shedding phases in Fig. 7 and 8. The same spatio-temporal symmetry has been found to characterize the two-dimensional wake past a single cylinder and

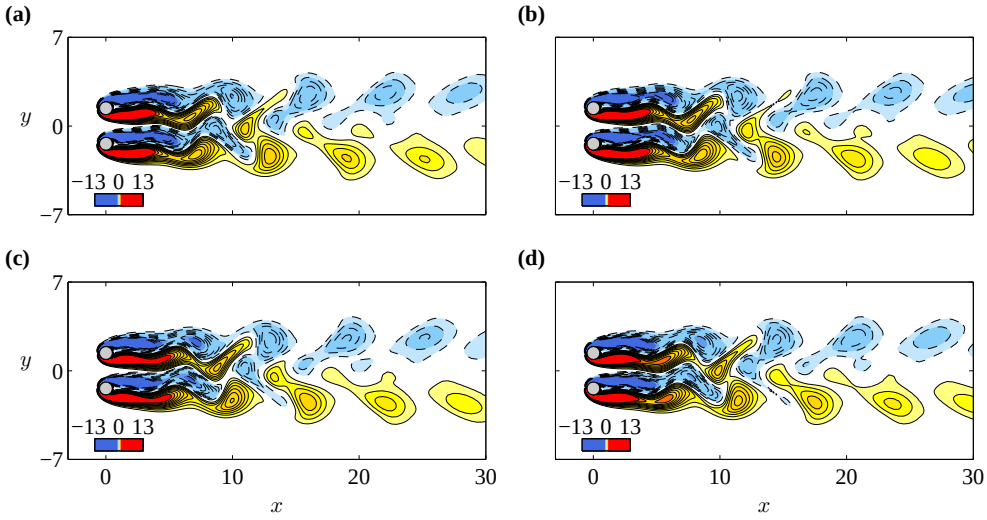

Figure 7: Vorticity snapshots of the periodic base flow for $g = 1.8$ and Re $= 54$. Four different shedding phases ϕ among the eight in which the base flow has been equally divided are illustrated: (a) $\phi = \pi/2$; (b) $\phi = \pi$; (c) $\phi = 3\pi/2$; (d) $\phi = 2\pi$.

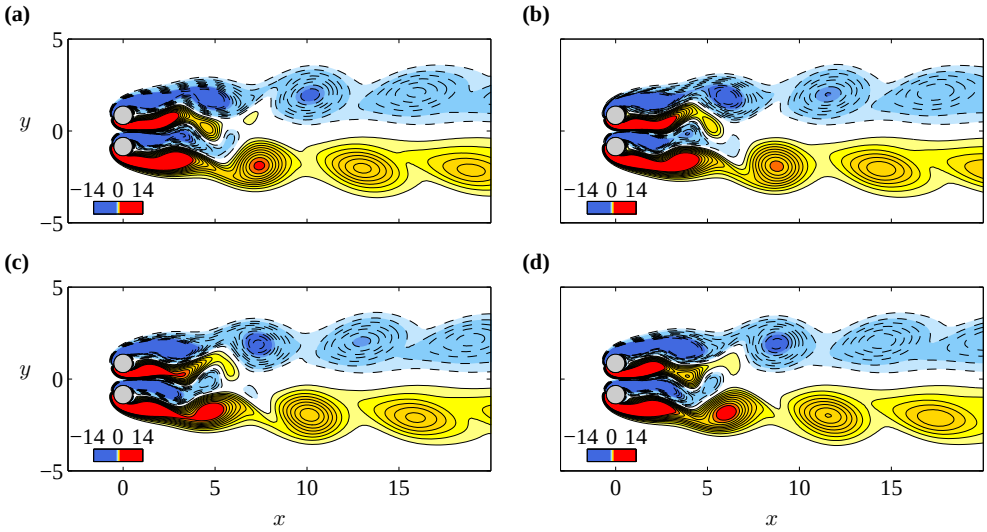

Figure 8: Vorticity snapshots of the periodic base flow for $g = 0.7$ and Re $= 61.6$. Four different shedding phases ϕ among the eight in which the base flow has been equally divided are illustrated: (a) $\phi = \pi/2$; (b) $\phi = \pi$; (c) $\phi = 3\pi/2$; (d) $\phi = 2\pi$.

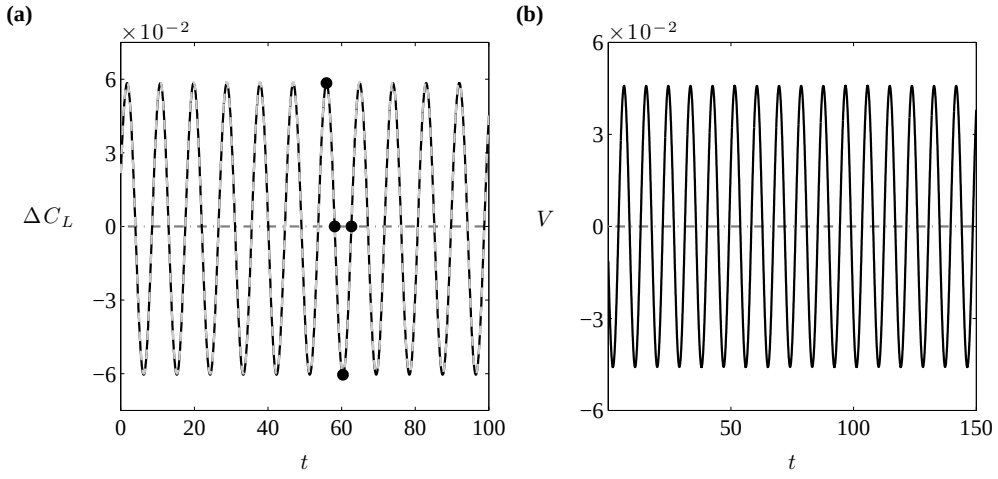

Figure 9: Periodic base flow for $g = 0.7$ and Re = 61.6. (a) Lift coefficient fluctuations $\Delta C_L = C_L - \bar{C}_L$ of the upper (black continuous line) and lower cylinder (dashed grey line); black dots are employed to mark shedding phases corresponding to the vorticity snapshots in Fig. 8. (b) Velocity component V of the flow field at $(x, y) = (0.5, 0)$ as a function of time.

following Robichaux et al. (1999) this symmetry is called reflectional-translation (RT):

$$\begin{cases} U(x, y, t) = U(x, -y, t + T/2), \\ V(x, y, t) = -V(x, -y, t + T/2). \end{cases} \tag{3}$$

In order to perform a Floquet analysis of the in-phase shedding cycle, the inherent periodic base flow has been computed for different values of Re in the neighbourhood of the critical flip-flop threshold which has been preliminarily estimated through DNS. The base flow Strouhal number St_b is plotted in Fig. 10(a) and 11(a) as a function of Re for $g = 0.7$ and $g = 1.8$, respectively. In particular, at supercritical Reynolds numbers, a suitable stabilization technique has to be employed to compute the periodic orbit. Several approaches can be adopted, such as the one devised by Lust et al. (1998) using the Recursive Projection method (Shroff and Keller, 1993). Another possibility is to use the Selective Frequency Damping method proposed by Akervik et al. (2006) (see also Viaud et al. 2011), provided that the frequency of the periodic base flow is well separated from the frequency of the unstable mode, as in the present case. In this paper a different approach has been employed for convenience. Basically our stabilization technique relies on a novel algorithm inspired by the Iterant Recombination method to accelerate fixed point iterations by correcting the next iteration with a linear combination of the previous ones (Trottenberg et al., 2001; Luchini, 2011). This algorithm is similar to a GMRES, but it is able to update with continuity the subspace of vectors used to get the new estimate.

5.2. The stability diagram

The linear stability of the in-phase shedding cycle has been first investigated for the two considered values of the gap spacing $g = 0.7$ and $g = 1.8$ at which DNSs were performed. In both cases the Floquet analysis indicates that a pair of complex-conjugate multipliers becomes unstable above the critical Reynolds number of Re ~ 61.74 for $g = 0.7$ and of Re ~ 51.72 for $g = 1.8$. The growth rate $\lambda = \mathrm{Re}(\sigma)$ and the frequency $\mathrm{St} = \mathrm{Im}(\sigma)/2\pi$ of the least stable Floquet exponent are plotted as a function of Re in Fig. 10 and 11 for $g = 0.7$ and $g = 1.8$, respectively. For both these cases, the computed values of St agree well with the lowest frequency peaks detected from DNS signals, Fig. 4, thus confirming that a Neimark–Sacker bifurcation of the in-phase periodic base flow lies at the root of the described flip-flopping behaviour. Moreover the Floquet mode at $g = 1.8$ becomes stable again for Re $\gtrsim 59.84$, Fig. 11(b), indicating that the linear instability of the in-phase periodic base flow at $g = 1.8$ is limited to a small range of Reynolds numbers. In our simulations at $g = 1.8$ the flip-flopping behaviour is still present for Re > 60 up to Re ≈ 65, while for Re $\gtrsim 65$ the in-phase base flow is restored, which is in agreement with Kang (2003) results. This

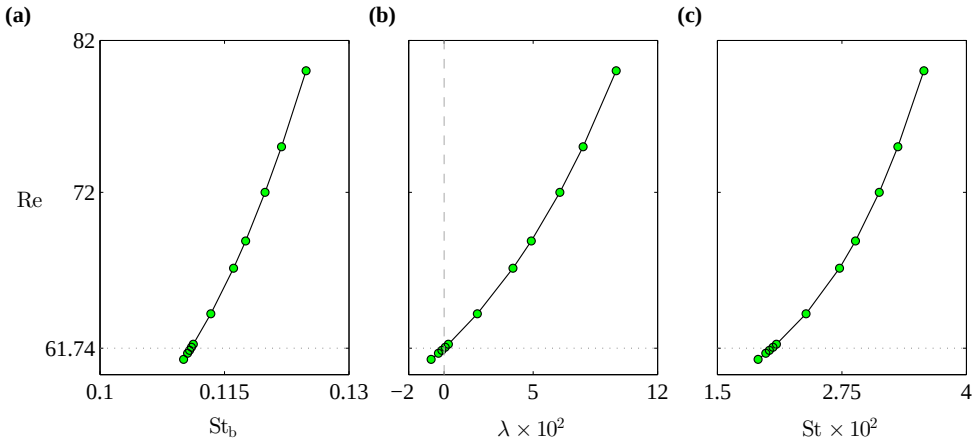

Figure 10: Floquet stability results as a function of Re for $g = 0.7$. (a) Periodic base-flow Strouhal number St_b. (b) Leading Floquet mode growth rate $\lambda = \mathrm{Re}(\sigma)$. (c) Leading Floquet mode frequency $\mathrm{St} = \mathrm{Im}(\sigma)/2\pi$.

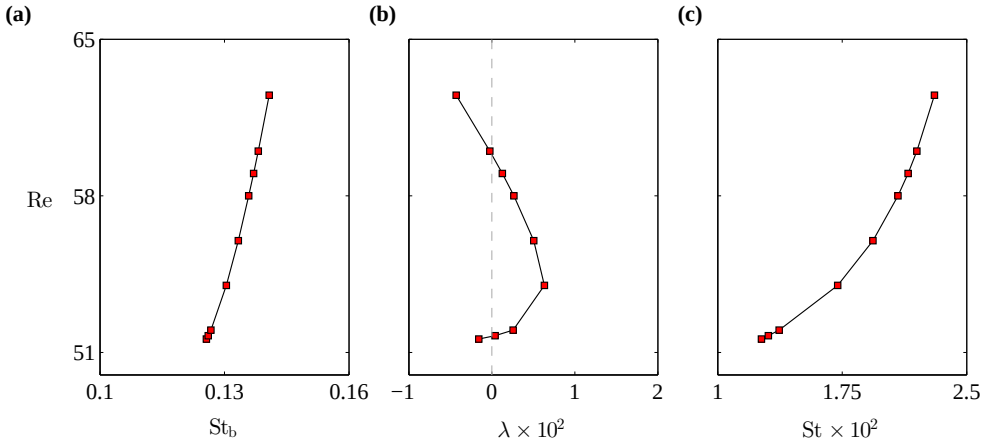

Figure 11: Floquet stability results as a function of Re for $g = 1.8$. (a) Periodic base-flow Strouhal number St_b. (b) Leading Floquet mode growth rate $\lambda = \mathrm{Re}(\sigma)$. (c) Leading Floquet mode frequency $\mathrm{St} = \mathrm{Im}(\sigma)/2\pi$.

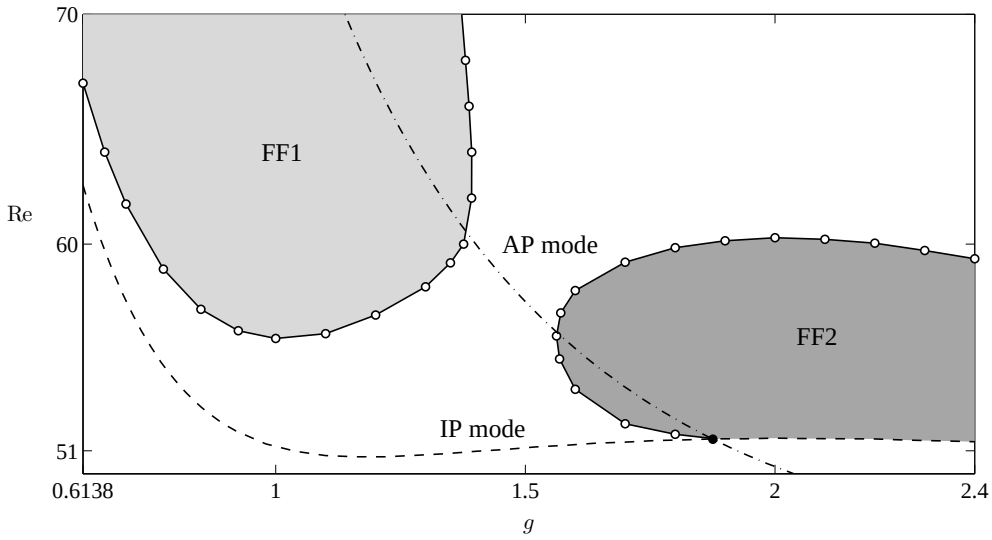

Figure 12: Neutral stability curves associated with the two unstable Floquet modes of the in-phase limit cycle. The grey shaded areas are used to denote the region of linear instability of the periodic base flow. The dashed and dash-dotted lines correspond to the neutral curves associated with the unstable IP and AP modes on the steady symmetric base flow, respectively. The round black dot indicates the double Hopf codimension-two bifurcation point at the intersection of the IP and AP neutral branches.

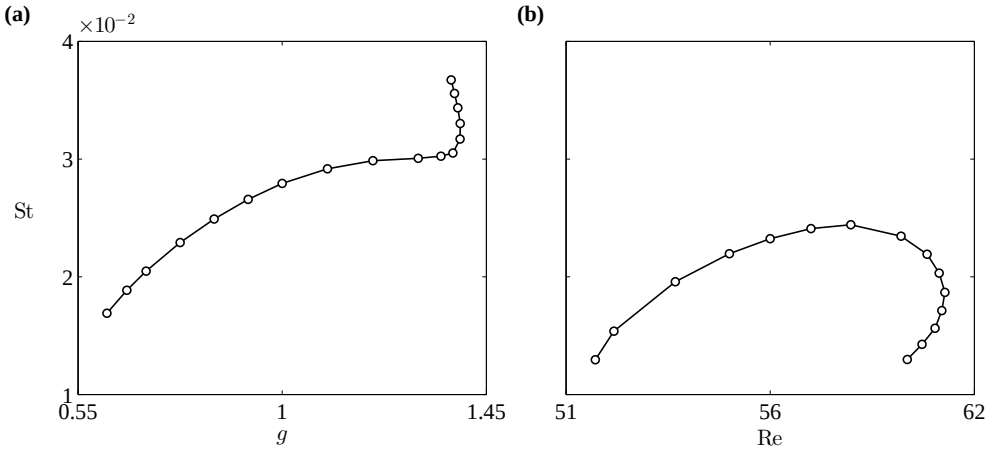

Figure 13: Variation of the leading Floquet mode frequency St = Im(σ)/2π along the neutral branches of Fig. 12. (a) St is plotted as a function of g along the FF1 branch. (b) St is plotted as a function of Re along the FF2 branch.

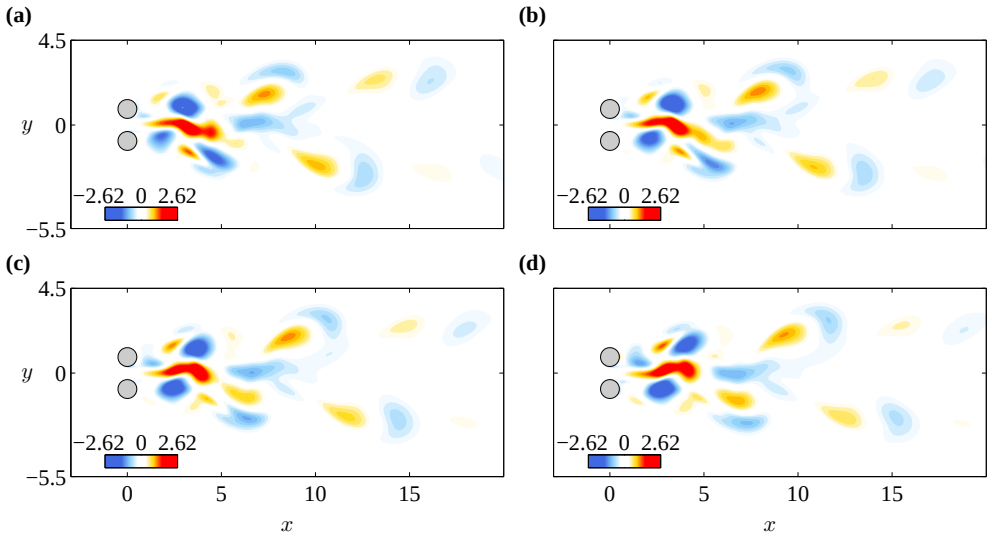

Figure 14: Vorticity field of the unstable direct Floquet mode $\hat{\boldsymbol{u}}(x, y, t)$ (real part) at $g = 0.7$ and $\mathrm{Re} = 61.8$. Pictures illustrate four subsequent shedding phases ϕ among the eight in which the periodic base flow has been equally divided: (a) $\phi = 0$; (b) $\phi = \pi/4$; (c) $\phi = \pi/2$; (d) $\phi = 3\pi/4$.

suggests that for $g = 1.8$ the upper bound of the instability domain is associated with a subcritical Neimark–Sacker bifurcation.

Starting from these results, the Floquet stability analysis has been extended to the region $0.6 \lesssim g \leq 2.4$ and $51 \leq \mathrm{Re} \leq 70$ in the parameter plane, tracking the critical Reynolds number threshold associated with the leading Floquet mode. The resulting neutral curves are depicted in Fig. 12. The neutral curves associated with the In-Phase (IP) and Anti-Phase (AP) oscillatory modes, which develop on top of the steady symmetric base flow are also reported in the same diagram (Carini et al., 2014b). These linear global modes are indeed responsible for the onset of the corresponding synchronized vortex shedding regimes (Akinaga and Mizushima, 2005; Mizushima and Ino, 2008). In particular, for $g \gtrsim 1.875$, the in-phase limit cycle becomes unstable just above the IP curve where it exists as a periodic solution of the governing equations (1). Two distinct domains of instability, highlighted by the grey shaded areas in Fig. 12, are described, namely FF1 and FF2. These results agree very well with the parameter region where the flip-flop has been observed by Kang (2003) by means of DNS. In particular the occurrence of the flip-flop for $g \approx 1.4-1.5$, in the intermediate region between FF1 and FF2, reported by Kang and confirmed in our DNS investigations, suggests that a subcritical behaviour occurs also in this region. However a detailed analysis of the subcritical nature of the Neimark-Sacker bifurcation is beyond the scope of the present analysis. In addition in Fig. 13, the variation of the leading Floquet mode frequency St along the two neutral branches of Fig. 12 is illustrated.

5.3. Direct Floquet mode at $g = 0.7$ and $g = 1.8$

The vorticity field associated with the real part of the direct Floquet mode $\hat{\boldsymbol{u}}(x, y, t)$ is illustrated in Fig. 14 and 15 for $g = 0.7$ and $g = 1.8$, respectively. The mode snapshots correspond to the phase angles $\phi = 0, \pi/4, \pi/2, 3\pi/4$ of the lift coefficient fluctuations, 2π representing a full cycle. Both unstable modes display a spatio-temporal symmetry which is opposite with respect to the symmetry of the periodic base flow, namely $\hat{u}(x, y, t) = -\hat{u}(x, -y, t + T/2)$, $\hat{v}(x, y, t) = \hat{v}(x, -y, t + T/2)$. This allows one to easily recover the portrait of the phases that are not shown here starting from the ones that have been reported.

For $g = 0.7$ and $\mathrm{Re} = 61.8$, the time-periodic perturbation field, Fig. 14, appears mainly concentrated in the near-wake region, with an irregular vortex shedding pattern developing behind the two cylinders and a strong vortical structure being formed in the region between the two cylinder wakes. The sign of this vortical structure is constant during a shedding period T and changes with the same frequency of the Floquet exponent. Furthermore, a shedding like mechanism takes place at the downstream edge of this region and a counter-clockwise rotating vortex is alternatively shed on each cylinder side during the in-phase shedding cycle. This mechanism seems to be at the root of

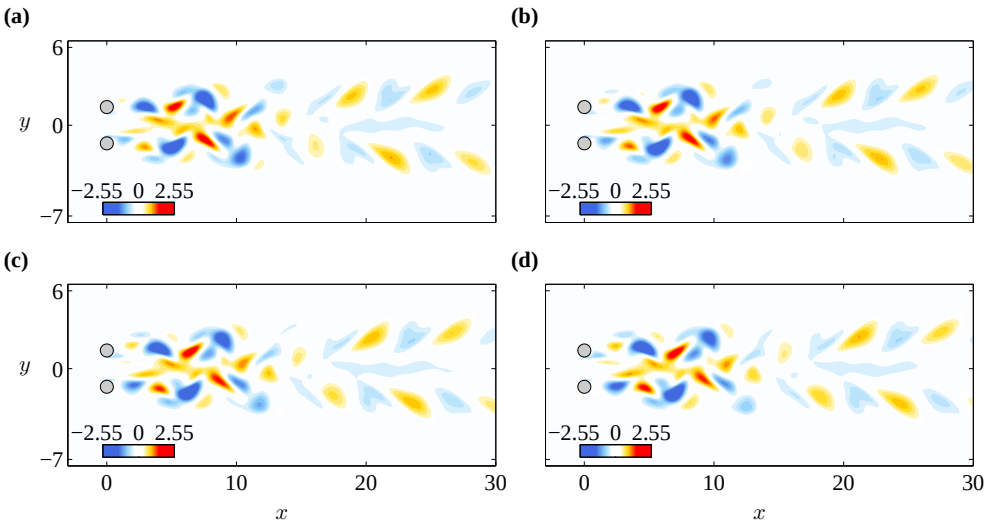

Figure 15: Vorticity field of the unstable direct Floquet mode $\hat{\boldsymbol{u}}(x, y, t)$ (real part) at $g = 1.8$ and $\mathrm{Re} = 54$. Pictures illustrate four subsequent shedding phases ϕ among the eight in which the periodic base flow has been equally divided: (a) $\phi = 0$; (b) $\phi = \pi/4$; (c) $\phi = \pi/2$; (d) $\phi = 3\pi/4$.

the biased merging process of gap eddies which characterizes the documented vortex dynamics in the flip-flopping regime at $g = 0.7$.

Conversely, for $g = 1.8$ and $\mathrm{Re} = 54$, Fig. 15, the mode structure extends far downstream from the two cylinders, with the region of maximum intensity being located at $\approx 5 - 6$ diameters from the cylinder centres. Two irregular vortex rows displaying an approximately anti-phase pattern are observed with a region of smaller intensity between them for $x \gtrsim 10$. Also in this case the sign of these vortical structures changes with the same frequency of the Floquet exponent, being constant over the shedding period T.

5.4. Weakly nonlinear analysis

The existence of a codimension-two Hopf-Hopf bifurcation point on the boundary of the flip-flop instability domain FF2 at $g_c = 1.875$ and $\mathrm{Re}_c = 51.51$ where the IP and AP neutral curves intersect (Carini et al., 2014b), see Fig. 12, motivates us to investigate the related phase-portrait based on classical bifurcation theory (Kuznetsov, 1998). Indeed it is known that higher-codimension bifurcations play an important role as 'organizing centres' of the system dynamics in their neighbourhood (Wiggins, 2003). For the considered bifurcation, the normal form reads

$$\begin{cases} \dfrac{dA}{dt} = \sigma_A(\epsilon, g)A + \nu_{AB}A|B|^2 + \nu_{AA}A|A|^2, \\ \dfrac{dB}{dt} = \sigma_B(\epsilon, g)B + \nu_{BA}B|A|^2 + \nu_{BB}B|B|^2, \end{cases} \tag{4}$$

where $A(t)$ and $B(t)$ denote the complex critical amplitudes associated with the IP and AP modes, respectively, and ϵ is the reduced Reynolds number, i.e. $\epsilon = (\mathrm{Re} - \mathrm{Re}_c)/\mathrm{ReRe}_c$. The coefficients $\sigma_A(\epsilon, g)$ and $\sigma_B(\epsilon, g)$ provide a linear estimate to the IP and AP eigenvalues when the parameters Re and g are varied in a neighbourhood of the bifurcation point

$$\begin{aligned} \sigma_A(\epsilon, g) &= \lambda_A(\epsilon, g) + i\omega_A(\epsilon, g) = i\omega_{A,0} + \sigma_{A,\epsilon}\epsilon + \sigma_{A,g}(g - g_c), \\ \sigma_B(\epsilon, g) &= \lambda_B(\epsilon, g) + i\omega_B(\epsilon, g) = i\omega_{B,0} + \sigma_{B,\epsilon}\epsilon + \sigma_{B,g}(g - g_c), \end{aligned} \tag{5}$$

$\omega_{A,0}$ and $\omega_{B,0}$ being the global mode frequency at criticality. The above coefficients and the remaining ones in (4) have been computed by means of a centre-manifold reduction of the discretized Navier-Stokes equations using the technique recently described by Carini et al. (2014a) which allows to derive directly the reduced nonlinear system

$\omega_{A,0}$	$0.7892i$
$\omega_{B,0}$	$0.8620i$
$\sigma_{A,\epsilon}$	$11.2833 + 4.5801i$
$\sigma_{B,\epsilon}$	$11.1258 + 4.2280i$
$\sigma_{A,g}$	$-1.4049 \times 10^{-3} + 2.6793 \times 10^{-2}i$
$\sigma_{B,g}$	$4.5347 \times 10^{-2} - 3.3647 \times 10^{-2}i$
ν_{AA}	$-9.5516 \times 10^{-4} + 4.7776 \times 10^{-3}i$
ν_{AB}	$-6.3149 \times 10^{-3} + 3.5165 \times 10^{-3}i$
ν_{BB}	$-3.6417 \times 10^{-4} + 1.8609 \times 10^{-3}i$
ν_{BA}	$3.2224 \times 10^{-3} + 8.4219 \times 10^{-3}i$

Table 2: Computed values of the normal-form coefficients for the double Hopf IP-AP bifurcation at $(g_c, \mathrm{Re}_c) = (1.875, 51.51)$ in the flow past two side-by-side cylinders.

in its normal form. The values of these coefficients are reported in Table 2. By introducing the polar coordinate transformation $A(t) = r_A(t)e^{i\phi_A(t)}$ and $B(t) = r_B(t)e^{i\phi_B(t)}$, the system (4) can be re-written in the form

$$\begin{cases} \dfrac{dr_A}{dt} = \lambda_A(\epsilon, g)r_A + \Re\{\nu_{AB}\}r_A r_B^2 + \Re\{\nu_{AA}\}r_A^3, \\ \dfrac{dr_B}{dt} = \lambda_B(\epsilon, g)r_B + \Re\{\nu_{BA}\}r_B r_A^2 + \Re\{\nu_{BB}\}r_B^3, \\ \dfrac{d\phi_A}{dt} = \omega_A(\epsilon, g), \\ \dfrac{d\phi_B}{dt} = \omega_B(\epsilon, g), \end{cases} \tag{6}$$

where terms of order $o(1)$ in the last two equations have been dropped according to the bifurcation analysis described by Kuznetsov (1998). Based on the computed values of the normal-form coefficients, the present situation falls in the subcase "III" of the 'simple' case in the classification reported by this author. In this case, the bifurcation diagram of (6) is completely determined by that of the planar system which consists of the first two equations, while the remaining equations simply describe rotations in the planes $r_A = 0$ and $r_B = 0$. Let us denote by $\boldsymbol{r} = (r_A, r_B)^T$ the reduced state vector collecting the modulus of A and B, for all values of the parameters Re, g the system (6) admits the trivial equilibrium point at the origin, i.e. $\boldsymbol{r}_0 = \boldsymbol{0}$ which corresponds to the steady symmetric base flow. Two other trivial equilibria are found for $\boldsymbol{r}_1 = (\bar{r_A}, 0)^T$ and $\boldsymbol{r}_2 = (0, \bar{r_B})^T$ which correspond to the in-phase and to the anti-phase vortex shedding limit cycles, respectively. In addition, a third non-trivial equilibrium $\boldsymbol{r}_3 = (\bar{\boldsymbol{r}_A}, \bar{\boldsymbol{r}_B})$ may also exist which generates a two-dimensional torus in the reduced four-dimensional phase-space. According to the related bifurcation diagram, the parameter plane in the neighbourhood of the codimension-two bifurcation point can be roughly partitioned into five regions which are illustrated in Fig. 16. In the same figure the two thick lines represent the neutral curve branches associated with the IP and AP modes. A different phase-portrait is associated with each region:

(1) only $\boldsymbol{r}_0$ exists which is a stable node;

(2) both $\boldsymbol{r}_0$ and $\boldsymbol{r}_1$ exist, $\boldsymbol{r}_0$ being a saddle and $\boldsymbol{r}_1$ a stable node;

(3) both $\boldsymbol{r}_0$ and $\boldsymbol{r}_2$ exist, $\boldsymbol{r}_0$ being a saddle and $\boldsymbol{r}_2$ a stable node;

(4) three equilibria exist: $\boldsymbol{r}_0$, $\boldsymbol{r}_1$ and $\boldsymbol{r}_3$, $\boldsymbol{r}_0$ and $\boldsymbol{r}_1$ being saddles and $\boldsymbol{r}_3$ a stable node;

(5) three equilibria exist: $\boldsymbol{r}_0$, $\boldsymbol{r}_1$ and $\boldsymbol{r}_2$, $\boldsymbol{r}_0$ being a source, $\boldsymbol{r}_1$ a saddle and $\boldsymbol{r}_2$ a stable node;

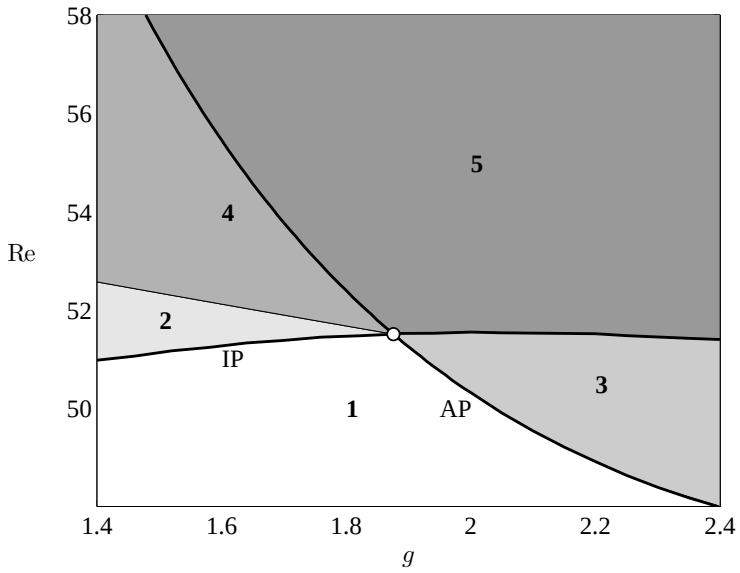

Figure 16: Bifurcation diagram resulting from the analysis of the normal form (4) related to the considered codimension-two Hopf-Hopf bifurcation (white dot). Black thick lines indicate the neutral branches associated with the IP and AP global modes.

An additional region is defined in the theoretical bifurcation diagram described by Kuznetsov (1998). With reference to Fig. 16, this region, i.e. the region 6, corresponds to a portion of the parameter space where both the IP and AP eigenmodes are unstable, being separated by the region 5 through an additional bifurcation curve originating from the codimension-two bifurcation point. In the region 6 all the four introduced equilibria exist, with $\boldsymbol{r}_0$ being a source, $\boldsymbol{r}_1$ and $\boldsymbol{r}_2$ being saddles and $\boldsymbol{r}_3$ a stable node. However, in the present case, the bifurcation curve separating region 5 and 6 nearly collapses on the AP neutral branch, with the region 6 being limited to a very narrow stripe near the AP upper branch.

The phase portrait described by the codimension-two bifurcation analysis is consistent with the results of the linear stability analysis reported in Fig. 12 for $g > 1.5$. In fact, both the Floquet stability and the normal-form analysis indicate that the bifurcation curve which leads to the quasiperiodic regime lies between the IP and AP neutral branches for $g < g_c$ while for $g > g_c$ the in-phase limit cycle becomes unstable in the region 5. This agreement suggests also that, in the region FF2, the flip-flop behaviour may be related to a nonlinear interaction between the IP and the AP modes. A similar conjecture for the appearance of the asymmetric modes at large g was proposed by Le Gal et al. (1990) based on the linear combination of the in-phase and anti-phase oscillations which results in beating-like waveforms.

It is interesting to note that the normal form (4) shares some features with the coupled oscillator model proposed and investigated by Le Gal et al. (1994) and by Peschard and Le Gal (1996). This low-dimensional model consists of two Landau equations associated with two identical oscillators, i.e. two cylinder wakes, which are coupled through additional linear terms

$$\begin{cases} \dfrac{d\tilde{A}}{dt} = \tilde{A} - (1 + ic_2)\tilde{A}|\tilde{A}|^2 + \dfrac{\eta}{\epsilon}(1 + ic_1)(\tilde{B} - \tilde{A}), \\ \dfrac{d\tilde{B}}{dt} = \tilde{B} - (1 + ic_2)\tilde{B}|\tilde{B}|^2 + \dfrac{\eta}{\epsilon}(1 + ic_2)(\tilde{A} - \tilde{B}). \end{cases} \tag{7}$$

In the above equations η/ϵ represents the magnitude of the coupling between the two cylinder wakes which is inversely proportional to the reduced Reynolds number and increases when reducing the distance between the cylinders. In the present case, the complex amplitudes $\tilde{A}$ and $\tilde{B}$ can be associated with the IP and AP critical amplitudes. It can be noticed that the universal value of c_2 is approximately the same for both the IP and the AP modes, with $c_{2,A} = \Im\{\nu_{AA}\}/\Re\{\nu_{AA}\} = -5.002$ and $c_{2,A} = \Im\{\nu_{AA}\}/\Re\{\nu_{AA}\} = -5.110$, as assumed in the coupled oscillator model.

These values are greater in magnitude than the value of $c_2 = -3.62$ computed for the first Hopf bifurcation of the cylinder wake (Carini et al., 2014a), which is in good agreement with those obtained by Sipp and Lebedev (2007) and by Meliga and Chomaz (2011), and also greater than the values tested by Peschard and Le Gal (1996). At the same time, the linear coupling terms in (7) are not present in the double Hopf normal form by construction. On the contrary, in (4), the coupling between the two oscillators is given by the third-order terms $A|B|^2$ and $B|A|^2$. It can be shown that in the coupled oscillator model, these latter terms can be recovered by introducing a linear coordinate transformation in order to diagonalize the linear part of the model. However, by means of such change of coordinates, additional third-order terms of the form B^*A^2 and $B|A|^2$ are also introduced which are not present in (4). These terms are responsible for a nonlinear behaviour richer than that of the double Hopf normal form, the significance of the latter being limited to a neighbourhood of the codimension-two bifurcation point. The comparison between the numerical solutions obtained from the coupled oscillator model varying the three parameters c_1, c_2 and η/ϵ and the experimental flow visualizations described by Peschard and Le Gal (1996) indicates that the model can reproduce several flow behaviours. Among these behaviours, the appearance of a quasiperiodic state in the transition region between the in-phase and in-phase locked solutions shows a clear analogy with the present Floquet stability results for $g \gtrsim 1.5$.

6. Conclusions

The two-dimensional secondary instabilities of the in-phase synchronized vortex shedding from two side-by-side circular cylinders have been herein investigated, providing a new rationale for the emerging of the flip-flopping behaviour of the cylinder wakes at low Reynolds numbers. By means of DNS and stability analyses, two different mechanisms for the flip-flopping have been identified at $g = 0.7$ and $g = 1.8$. For $g = 0.7$, the flip-flop instability is shown to break the RT-symmetric merging process of small gap eddies into the outer wake (which characterizes the corresponding in-phase base flow) resulting in the biased amalgamation of both eddies toward the same side of the outer wake for more than one shedding cycle. Conversely for $g = 1.8$ the flip-flopping instability is found to inhibit the formation of the binary vortex street pattern, by preventing like-sign vortex pairing on one side of the wake but not on the other side. In both cases the two-dimensional Floquet stability analysis of the related in-phase shedding cycle, shows that a pair of complex-conjugate modes becomes unstable at fairly low Reynolds numbers, i.e. $\mathrm{Re} \approx 61.74$ for $g = 0.7$ and $\mathrm{Re} = 51.72$ for $g = 1.8$. Two distinct domains of Floquet instability in the parameter plane (g, Re) are described, showing very good agreement with the results obtained by Kang (2003) by means of DNS. Although complicated, the spatio-temporal structure of the two Floquet modes shows strong analogies with the corresponding flip-flop mechanism. Furthermore the associated eigenvalue frequency agrees well with the lowest St peak extracted from DNS analysis, which is associated with the gap flow switchover.

These results clearly support the proposed bifurcation scenario for the emerging of the flip-flop compared to the bi-stability interpretation conjectured by other authors. This scenario is consistent with the existence of different flip-flop mechanisms at moderate and large gap spacing, a fact which is pointed out here for the first time, to the authors' knowledge. Furthermore, the weakly nonlinear analysis performed in the neighbourhood of the IP-AP codimension-two bifurcation point indicates that the quasiperiodic behaviour associated with the flip-flop at large gap spacing may be related to the nonlinear interaction between the two synchronized shedding modes.

Finally, we note that a clear connection between the low and high Re flip-flop regimes cannot be stated based on the present results since the present analysis is restricted to very low Reynolds numbers and it is likely that other transitions appear at higher Re.

References

Afgan, I., Kahil, Y., Benhamadouche, S., Sagaut, P., 2011. Large eddy simulation of the flow around single and two side-by-side cylinders at subcritical Reynolds numbers. Phys. Fluids 23, 1–17.

Akervik, E., Brandt, L., Henningson, D.S., Hoepffner, J., Marxen, O., Schlatter, P., 2006. Steady solutions of the Navier-Stokes equations by selective frequency damping. Phys. Fluids 18, 068102.

Akinaga, T., Mizushima, J., 2005. Linear stability of Flows past Two Circular Cylinders in a Side-by-Side Arrangement. J. Phys. Soc. Japan 74, 1366–1369.

Bearman, P.W., Wadcock, A.J., 1973. The interaction between a pair of circular cylinders normal to a stream. J. Fluid Mech. 61, 499–511.

Camarri, S., Giannetti, F., 2010. Effect of confinement on three-dimensional stability in the wake of a circular cylinder. J. Fluid Mech. 642, 477–487.

Carini, M., Auteri, F., Giannetti, F., 2014a. Centre-manifold reduction of bifurcating flows. Submitted to J. Fluid Mech.
Carini, M., Giannetti, F., Auteri, F., 2014b. First instability and structural sensitivity of the flow past two side-by-side cylinders. J. Fluid Mech. 749, 627–648.
Chen, L., Tu, J.Y., Yeoh, G.H., 2003. Numerical simulation of turbulent wake flows behind two side-by-side cylinders. J. Fluids Struct. 18, 387–403.
Davis, T.A., 2004. Algorithm 832: UMFPACK, an unsymmetric-pattern multifrontal method. ACM Trans. Math. Software 30, 196–199.
Giannetti, F., Camarri, S., Luchini, P., 2010. Structural sensitivity of the secondary instability in the wake of a circular cylinder. J. Fluid Mech. 651, 319–337.
Giannetti, F., Luchini, P., 2007. Structural sensitivity of the first instability of the cylinder wake. J. Fluid. Mech. 581, 167–197.
Kang, S., 2003. Characteristics of flow over two circular cylinders in a side-by-side arrangement at low reynolds numbers. Phys. Fluids 15, 2486–2498.
Kim, H.J., Durbin, P.A., 1988. Investigation of the flow between a pair of circular cylinders in the flopping regime. J. Fluid Mech. 196, 431–448.
Kuznetsov, Y.A., 1998. Elements of applied bifurcation theory. 2nd ed., Springer.
Le Gal, P., 1991. Chaos spatio-temporel dans une chaîne de sillages couplés. C. R. Acad. Sci. Paris 313, 1499–1506.
Le Gal, P., Chauve, M.P., Lima, R., Rezende, J., 1990. Coupled wakes behind two circular cylinders. Phys. Rev. A 41, 4566–4569.
Le Gal, P., Chauve, M.P., Peschard, I., Jarre, S., 1994. The Ginzburg-Landau equation and the transition to turbulence in open flows. Current Topics in The Physics of Fluids 1, 307–318.
Lehoucq, R.B., Sorensen, D.C., Yang, C., 1998. ARPACK Users Guide. siam ed.
Luchini, P., 2011. Private communication.
Lust, K., Roose, D., Spence, A., Champneys, A.R., 1998. An adaptive Newton-Picard algorithm with subspace iteration for computing periodic solutions. SIAM J. Sci. Comp. 19, 1118–1209.
Meliga, P., Chomaz, J.M., 2011. An asymptotic expansion for the vortex-induced vibrations of a circular cylinder. J. Fluid Mech. 671, 137–167.
Mizushima, J., Ino, Y., 2008. Stability of flows past a pair of circular cylinders in a side-by-side arrangement. J. Fluid Mech. 595, 491–507.
Peschard, I., Le Gal, P., 1996. Coupled wakes of cylinders. Phys. Rev. Lett. 77, 3122–3125.
Rai, M.M., Moin, P., 1991. Direct simulations of turbulent flow using finite-difference schemes. J. Comp. Phys. 96, 15–53.
Robichaux, J., Balanchadar, S., Vanka, S.P., 1999. Three-dimensional Floquet instability of the wake of a square cylinder. Phys. Fluids 11, 560–578.
Shroff, G.M., Keller, H.B., 1993. Stabilization of unstable procedures: the recursive projection method. SIAM J. Numer. Anal. 30, 1099–1120.
Sipp, D., Lebedev, A., 2007. Global stability of base and mean flows: a general approach and its applications to cylinder and open cavity flows. J. Fluids Mech. 593, 333–358.
Sumner, D., 2010. Two circular cylinders in cross-flows: A review. J. Fluids Struct. 26, 849–899.
Sumner, D., Wong, S.S.T., Price, S.J., Païdoussis, M.P., 1999. Fluid behavior of side-by-side circular cylinders in steady cross-flow. J. Fluids Struct. 13, 309–338.
Trottenberg, U., Oosterlee, C., Schüller, A., 2001. Multigrid. Academic Press.
Viaud, B., Serre, E., Chomaz, J.M., 2011. Transition to turbulence through steep global-modes cascade in an open rotating cavity. J. Fluid Mech. 688, 493–506.
Wang, Z.J., Zhou, Y., Li, H., 2002. Flow-visualization of a two side-by-side cylinder wake. J. Flow Visual. & Image Proces. 9, 123–138.
Wiggins, S., 2003. Introduction to applied nonlinear dynamical systems and chaos. Springer.
Williamson, C.H.K., 1985. Evolution of a single wake behind a pair of bluff bodies. J. Fluid Mech. 159, 1–18.
Zdravkovich, M.M., 1977. Review of flow interference between two circular cylinders in various arrangement. Trans. ASME I: J. Fluids Engng 99, 618–633.
Zhou, Y., Zhang, H.J., Yiu, M.W., 2002. The turbulent wake of two side-by-side circular cylinders. J. Fluid Mech. 458, 303–332.